ELSEVIER

Fiber-Matrix Interaction in Microfiber-Reinforced Mortar

L.R. Betterman,* C. Ouyang,† and S.P. Shah‡
*Larson Engineering, Minneapolis, Minnesota, †Office of Materials, Iowa Department of Transportation, Ames, Iowa, and ‡National Science Foundation Center for Advanced Cement Based Materials, Northwestern University, Evanston, Illinois

The tensile properties of mortar reinforced with polyvinyl alcohol (PVA) fibers were studied in this article. Specimens reinforced with varying volume fractions of different-sized fibers were tested in direct tension. Pull-out tests were also conducted to evaluate the interfacial properties between the PVA fiber and mortar matrix. In addition, scanning electron microscopy was used to study the failure mechanism of the fibers in the direct tension test specimens. To study fiber distribution, images of the specimen cross-sections obtained with an optical microscope were analyzed. It was found that if the influence of fiber length is taken into account, the first peak stress can be expressed as a unique function of the measured fiber distance, regardless of fiber volume fraction and diameter. ADVANCED CEMENT BASED MATERIALS 1995, 2, 53–61

KEY WORDS: Bond, Cement, Composite materials, Concrete, Fibers, Fracture, Microscopy, Reinforcement, Tensile properties

The recent interest in the use of microfibers in cement based materials is motivated by the effect of fiber dimensions on the tensile properties of composite materials [1–7]. Consider a matrix reinforced with an identical volume and aspect ratio of large fibers and microfibers. For the volume of fibers normally used for cementitious composites, when relatively large fibers are used as reinforcement, only a small improvement in tensile strength is observed (Figure 1). This is probably due to the fact that matrix cracking first occurs at the micro level. If fibers are far apart, they have no ability to arrest microcracks. However, once the microcracks condense into macrocracks, the large fibers can arrest propagation macrocracks and substantially improve the toughness of the composite (Figure 1). If microfibers are used, they can bridge microcracks, since for a given volume these fibers are much closer together. Microfibers can thus significantly enhance the tensile strength of the composite as sketched in Figure 1. However, for the same aspect ratio, microfibers are shorter and therefore may be pulled out after macrocracks are formed, thus providing little improvement in post peak toughness. By combining fibers of varying sizes into the matrix, improvement in both the peak stress and post peak toughening can be expected.

This investigation focused on studying the tensile properties of a cement based mortar reinforced with varying volume fractions of different-sized polyvinyl alcohol (PVA) microfibers. Direct tension tests were performed on dog-bone-like specimens. The study was aimed at understanding the effect of both length and diameter of the fiber on the material properties. To investigate the bond between the matrix and fiber, pull-out tests were performed using continuous PVA fibers. Scanning electron microscopy and optical microscope imaging, respectively, were used to determine the failure mechanism and to quantify fiber distribution in the tensile specimens. The measured fiber distance was then related to mechanical properties of composites. For a given aspect ratio, the smaller the diameter, the shorter the length.

Experimental Program

Materials

The mortar matrix used in this study consisted of type I Portland cement and sand at a weight ratio of 1:1. In addition, 18% of silica fume by weight of cement was added, resulting in a water:binder ratio of 0.3. To improve workability and placement of the mix, superplasticizer (WRDA-19 Superplasticizer, Grace Construction Products) was added in high doses (3 to 5% by weight of cement).

Three different lengths (4, 7, and 12 mm) of cut, water-insoluble PVA fibers (produced by Kuraray Co., Ltd., Osaka, Japan) were used in this investigation. The diameter of fiber was varied so that each fiber length had an approximate aspect ratio of 300. Table 1 lists the properties of each fiber, including tensile strength, elongation, and modulus. The density of the PVA fiber was 1.3 g/cm^3.

Address correspondence to: S.P. Shah, Center for Advanced Cement Based Materials, Northwestern University, 2145 Sheridan Road, Room A130. Evanston, Illinois 60208.
Received February 9, 1994; Accepted June 8, 1994

ISSN 1065-7355/95/$9.50
SSDI 1065-7355(94)00027-B

Advn Cem Bas Mat
1995;2:53–61

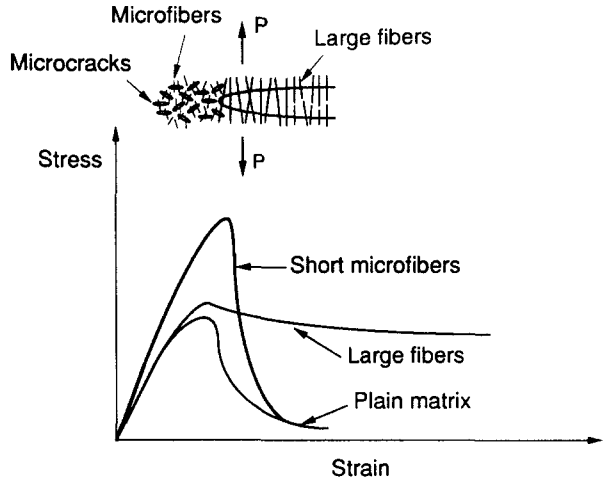

FIGURE 1. Illustration of different sizes of fibers on crack bridging.

Mixing Process

A total of 10 batches of PVA fiber-reinforced mortar were prepared for direct tension testing. Each of the three fiber lengths was mixed into the matrix at volume fractions of 1, 2, and 4%, for a total of nine batches. The tenth batch consisted of a mixture of 2% of the 4-mm fiber and 2% of the 12-mm fiber for a total fiber volume fraction of 4%. Table 2 summarizes the amount and size of fiber used in each batch. In addition, the same composition of mortar matrix was used to prepare the pull-out specimen.

All mixing was done in an OMNI Mixer (model OM-10E, Chiyoda Technical & Industrial Co., Ltd.). The unique feature of this mixer is that it does not induce any shear forces on the mixed material, as is done by a conventional blade mixer. The advantages of this mixer are that it will not cause damage to the fibers while mixing because of the absence of shear forces, and it will disperse fibers evenly throughout the mix because of its use of random motion.

It was determined that the following procedure gave the best results. The sand and cement were first mixed together for 1 minute on setting 10 (approximately 450 rpm). The water, silica fume slurry, and superplasticizer were then mixed together in a separate container by simply stirring. This reduces the stickiness of the silica fume slurry and aids in its dispersion. With the OMNI Mixer on setting 3 (approximately 205 rpm), the fluid mixture of water, silica fume slurry, and superplasticizer was slowly added over a 20-second period. After all of the fluid mixture was added, the OMNI Mixer was turned up to setting 7 (approximately 345 rpm) for 1 minute. The mixer was then turned down to setting 3 while the fibers were slowly sprinkled in over a 20-second period. Finally, the mixer was again turned up to setting 7 for 1 minute and then shut off. The total mixing time was approximately 4 minutes.

After mixing, the fresh mix was placed into the specimen molds (12 for each batch) by hand using a trowel. In addition, a vibrating table was used to achieve good compaction and to minimize the amount of the entrapped air within the mix. Once all 12 molds had been filled, they were covered with plastic and wet towels to keep the specimens from drying out. Approximately 24 hours later the specimens were removed from the molds and placed in a water bath until preparation for testing was to be done.

Less workability of the mix was experienced for the batches having a 4% volume fraction of fiber than for those with 1 and 2% volume fractions due to the higher quantities of fibers. As a result, additional amounts of superplasticizer were added to the mixtures having 4% volume fractions of fibers. Batches having fiber volume fractions of 1 and 2% received 3% (by weight of cement) of superplasticizer, while the batches having a 4% fiber volume fraction received 5% of superplasticizer.

Since lengths of the fiber used (4, 7, and 12 mm) are in the same order with the dimension of cross-section of the specimen (6 × 16 mm), it is expected that fibers are more or less aligned along the length direction of the specimen.

In addition, one batch of unreinforced mortar was prepared for casting of the pull-out test specimens. The mixing procedure was similar to that described above except that no fibers were added to the mortar matrix.

Direct Tension Test

Specimens for the direct tension test had cross-sectional dimensions of 16 × 9 mm and a length of 244 mm as shown in Figure 2. Approximately 14 days after casting, the specimens were removed from the water bath for surface grinding. Here the free-curing surface (the dog-bone-shaped surface that was not in contact with the mold) of each specimen was ground down parallel to its opposite surface using an automatic-feed, water-cooled, diamond wheel grinder. The specimens remained wet during grinding and were returned to the water bath immediately after grinding was completed. Approximately 5 days before testing, the specimens were again removed from the water bath in order to attach the end plates to them (see Figure 2). It was determined that the epoxy, Transpo T-55 (Transpo Industries Inc., New Rochelle, New York) gave the best performance in adhering the 0.127 mm mild steel end plates to the specimens.

A previously developed testing apparatus was used to carry out the direct tension test [5]. The apparatus

TABLE 1. Properties of the polyvinyl alcohol fibers

Length (mm)	Diameter (mm)	Aspect Ratio	Tensile Strength (GPa)	Elongation (%)	Elastic Modulus (GPa)
4	0.012	331	1.27	8.1	28.1
7	0.024	295	1.27	9.1	27.7
12	0.041	292	1.01	11.9	16.4

consisted of an 89-kN capacity closed-loop Materials Testing System (MTS) test machine equipped with a 22.25-kN load cell. Two rigid friction grips, one attached to the cross head and the other attached to the actuator piston, were used to mount the specimens within the load frame. Axial deformation of the specimens was measured using two 0.64-mm linear voltage differential tranducers (LVDTs) with a gauge length of 76 mm. The LVDTs were mounted on each side of the specimen with aluminum holders and rubber bands. The controlling variable was the average reading of the two LVDTs, ramped at a rate of 0.01524 mm/minute. Generally, tension tests were performed for each batch until at least four successful tests gave similar results.

Pull-Out Test

Fiber pull-out testing and specimen preparation followed a technique developed by Li et al. [8]. Specimens for the pull-out test were cast in a brass mold having cross-sectional dimensions of 25 × 57 mm. The testing apparatus used in the pull-out test consisted of an 89-kN capacity MTS closed-loop test machine equipped with a 4.45-kN load cell. To measure slip displacement, two extensometers with a range of 0.19 mm and a gauge length of 12.7 mm were mounted on both sides of the specimen. To control the test, the average readout of the two extensometers was used as the feedback signal. The fibers were pulled out at a constant slip rate of 0.000762 mm/second.

Results and Discussions

Direct Tensile Test

Typical stress-strain curves for the specimens with a fiber volume fraction of 2% and with fiber lengths of 4 or 12 mm are shown in Figure 3. Each curve approxi-

TABLE 2. Size and amount of fibers used in each batch and corresponding average values of first peak stress and strain energy density at 6000 με for ages of 1 and 3 months

Batch Label	Fiber Length (mm)	Fiber Volume Fraction (%)	Amount of Fiber Added (g)	Average First Peak Stress (MPa)	Average Energy at 6000 με (J/m^3)
D	4	2	60	2.33 (4.77)	6,997 (10,814)
E	7	2	60	2.64 (3.29)	11,825 (12,288)
F	12	2	60	1.42 (3.35)	14,771 14,263
G	4	1	30	0.82 (2.57)	2,987 (4,659)
H	7	1	30	0.80 (1.15)	5,448 (6,384)
I	12	1	30	— (1.23)	8,914 (10,318)
J	4	4	120	5.49 (4.21)	11,774 (17,658)
K	7	4	120	4.53 (3.98)	13,565 (9,131)
L	12	4	120	4.36 (3.89)	13,932 (17,847)
P	4 & 12	4	60 & 60	5.74	22,478

Three-month data appear in parenthesis.

Advn Cem Bas Mat
1995;2:53–61

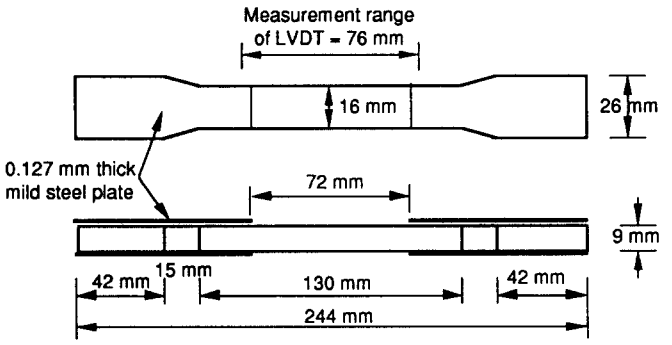

FIGURE 2. Direct tension test specimen.

mately contains an initial elastic region up to what is termed the first peak stress. After reaching the first peak stress, a sudden drop in stress is encountered, followed by a postpeak curve which may or may not exceed the first peak stress. The corresponding strain energy density curves, which are constructed by integrating the area under the stress-strain curves, are shown in Figure 4. To quantify the information given by the stress-strain and strain energy density curves, the values of first peak stress and strain energy density at 6000 μE were obtained. These values were then used to characterize the mechanical properties of the composite material. In determining the strain energy density values, it is noted that some estimation of strain energy density for specimens with 1% fiber volume fraction was done in the cases where a test was halted before reaching 6000 μE. This was done by simply extending the stress-strain curve with a line having a slope equal to that of the stress-strain curve until the line reached the 6000 μE level or zero stress. Since stress levels at the end of testing are usually very low, the estimation does not result in significant error. Average values of the first peak stress and the strain energy density at 6000 μE are listed in Table 2.

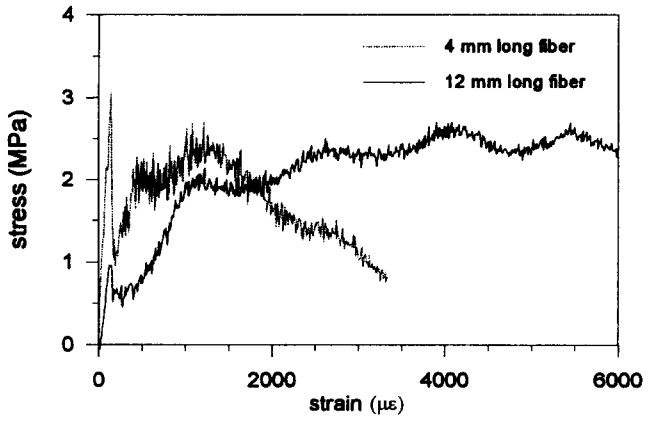

FIGURE 3. Typical stress-strain curves for a 2% volume fraction of 4-mm and 12-mm long fiber.

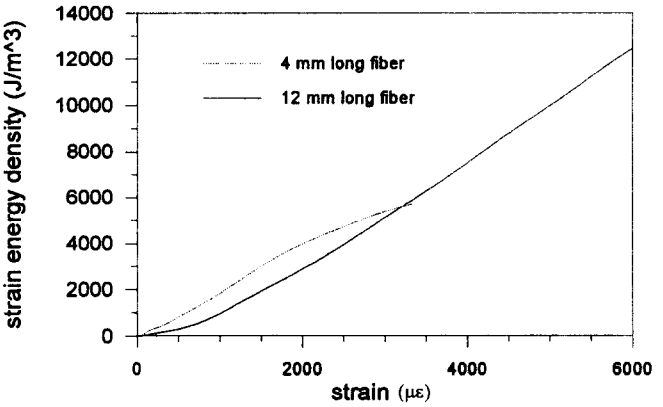

FIGURE 4. Typical strain energy density curves for a 2% volume fraction of 4-mm and 12-mm long fiber.

The first peak stress and the strain energy density at 6000 μE tested at the age of 3 months are plotted against fiber volume fraction for the 4-mm long fiber in Figure 5a and b, respectively. Both the first peak stress and the strain energy density increase with an increase in fiber volume fraction.

A relationship between first peak stress and fiber diameter is shown in Figure 6a for specimens having a 2% fiber volume fraction. It is noted that since the aspect ratio of each fiber is the same (approximately 300), the greater the diameter, the longer the fiber. From the figure, it is evident that first peak stress decreases as fiber diameter increases. This trend is also observed for specimens having fiber volume fractions of 1 and 4%. The plot of strain energy density at 6000 μE versus fiber diameter is given for specimens having a 2% fiber volume fraction in Figure 6b. It is observed that an increase in fiber diameter leads to an increase in strain energy density.

These results indicate that short, small-diameter fibers are more efficient in increasing the first peak stress. This may be due to the fact that opening and propagating of numerous microcracks are primarily responsible for the magnitude of the first peak stress. A large number of short, small-diameter fibers may effectively bridge these microcracks. On the other hand, a major crack forms after the first crack stress. Opening of the major crack is much greater than that of the microcrack, which may result in the pull-out of short, small fibers. As a result, bridging of the major crack is primarily provided by long fibers. This may explain why the longer the fiber, the greater the energy density.

Pull-Out Test

A typical load-slip curve from a specimen having an embedment length of 13 mm is shown in Figure 7, where the total pull-out load of 16 fibers is indicated.

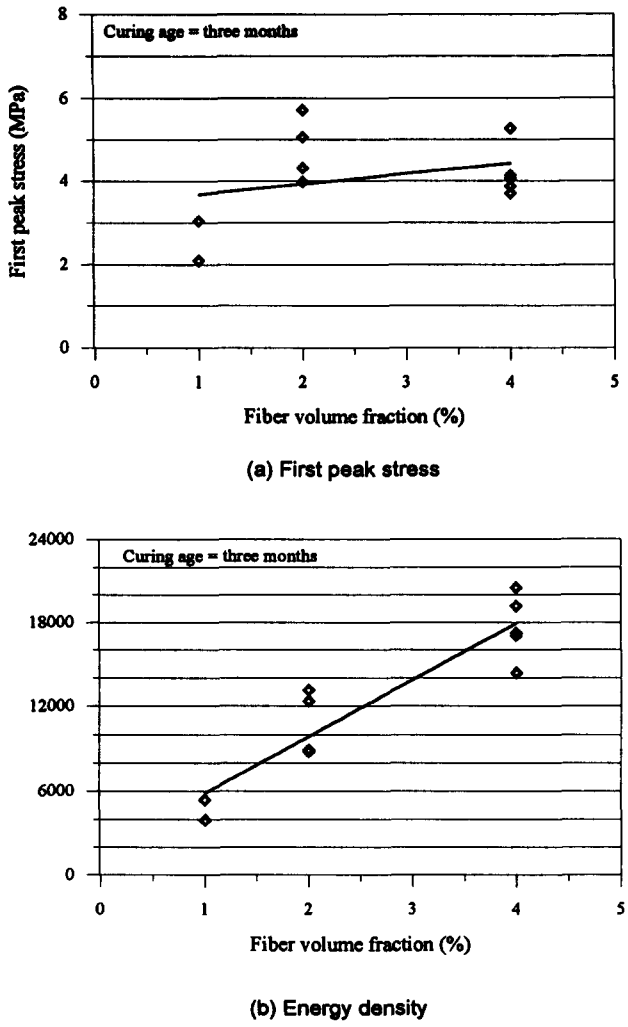

FIGURE 5. Influence of fiber volume fraction for 4-mm long fiber.

Initially, the pull-out load increases with the slip. Although the slope of the curve decreases at point A, the pull-out load still increases with the slip until the peak load (point B) is reached. Similar load-slip curves for pull-out of polypropylene and nylon fibers have been reported by Wang et al. [5].

A simple theoretical model proposed by Li et al. [8] was used to calculate the pull-out properties from the measured pull-out slip curves. The obtained results are listed in Table 3, where the shear stiffness of the fiber-matrix boundary layer (ω), the shear bond strength (τ_y), the frictional bond strength (τ_f), and the specific interfacial fracture energy (Γ) are included. For comparison, pull-out parameters for a steel fiber reported by Li et al. [8] are also given in Table 3. It is evident that the shear stiffness, shear bond strength, and frictional bond strength between the steel and PVA fibers are similar. However, the specific surface energy of the PVA fiber is much higher than that of steel.

Microscopic Investigation

To further investigate the interaction between the PVA fiber and mortar matrix, two microscopic observations were performed in this study. One consisted of observing fracture surfaces of tensile specimens using a scanning electron microscope to determine the fiber failure mechanism. The other consisted of observing fiber distribution on polished cross-sectional surfaces using an optical microscope to determine the influence of fiber distribution.

Specimen Preparation

A total of 10 specimens were chosen to be used in this microscopic investigation, one from each of the batches prepared for direct tension testing. Specimens were chosen having the most typical stress-strain curves of their batch, and having fracture locations that could be easily prepared for observation.

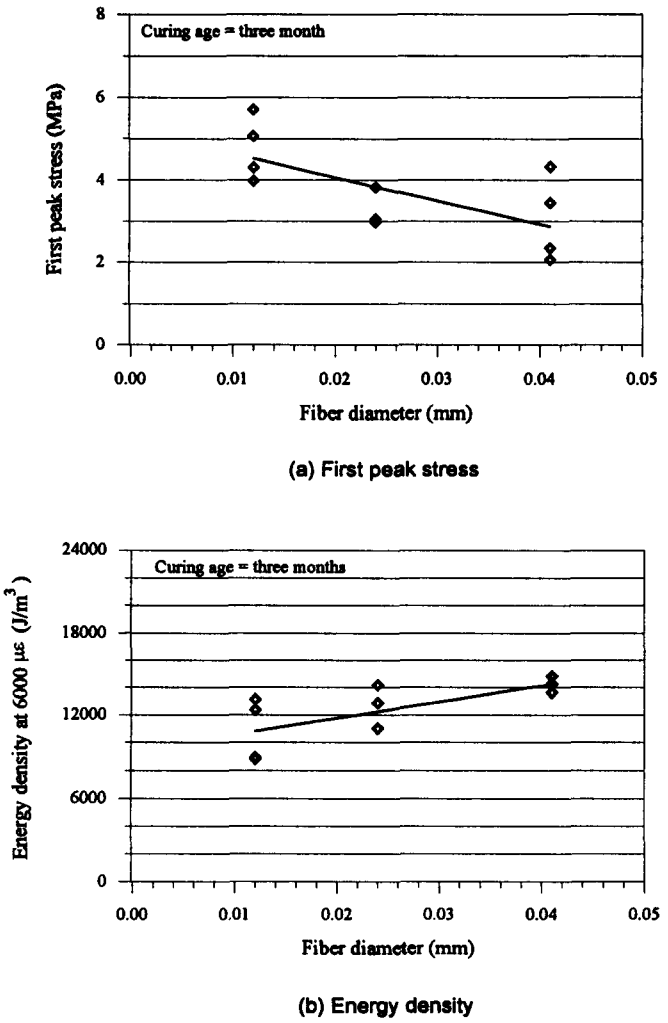

FIGURE 6. Influence of fiber diameter for 2% fiber volume fraction.

Advn Cem Bas Mat
1995;2:53–61

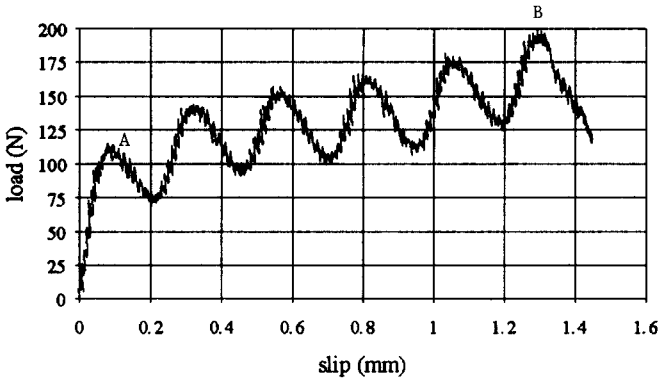

FIGURE 7. Typical load-slip curve from a PVA fiber pull-out test.

Fracture surfaces were prepared by simply cutting them off from the specimens with a diamond band saw after they had been fractured during direct tension testing. This cut was made parallel to the general direction of the fracture surface. The obtained sections were observed under a scanning electron microscope to determine the fiber failure mechanism.

Polished cross-sections were prepared by first cutting a 5-mm thick strip off of the direct tension specimens, just behind the fracture surface. The thin cross-sections were then cold-mounted in an epoxy (Sampl-Kwick, Buehler, Lake Bluff, Illinois). Polishing began by using a water-cooled polishing wheel rotated by an electric motor and equipped with various grits of sandpaper. Sandpapers having grits of 240, 320, and 600 were used in sequence. Final polishing was done using dry diamond-polishing wheels. One wheel had a 6-μm grit surface, while the other had a 1-μm grit surface. The obtained polished sections were observed using an optical microscope to determine fiber distribution.

Failure Mechanism of Fibers by Scanning Electron Microscopy

Fracture surfaces were observed with a scanning electron microscope (Hitachi S-570LB) to determine the failure mechanism the fibers had undergone during direct tension testing. Figure 8 shows a fiber from one of the fracture surfaces magnified 600 times. As can be seen, the fiber has pulled out of the matrix since there is no indication of fiber failure at its end. In addition,

TABLE 3. Fiber-matrix interfacial properties for PVA and steel fiber

Fiber Type	ω (m^{-1})	τ_y (MPa)	τ_f (MPa)	Γ (N/m)
PVA, T2	133	2.72	0.722	105
Steel (28 d.)	75	2.35	1.42	17.7

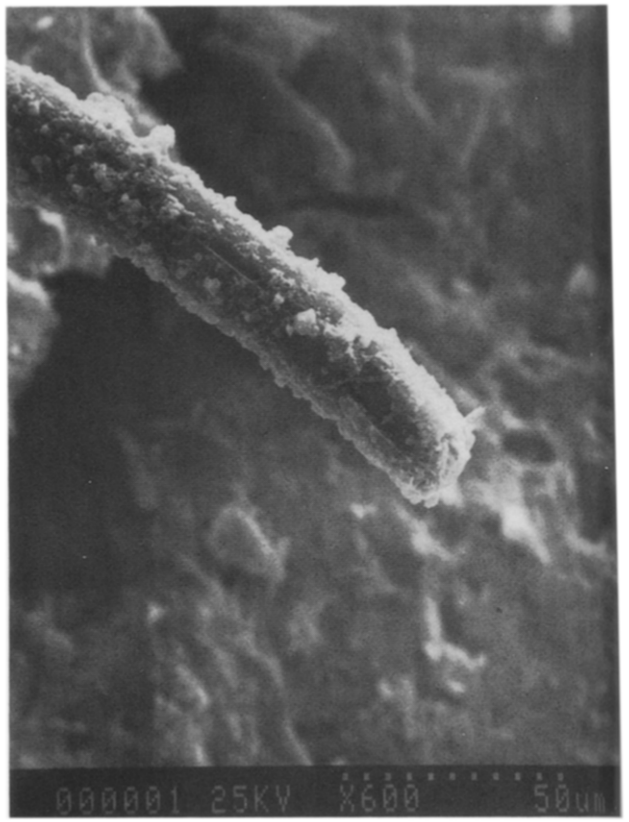

FIGURE 8. PVA fiber extending out from a fracture surface (600× magnification).

there are particles attached to the fiber, which indicates a good level of bond between the fiber and matrix. This can be compared to the smooth surface of a fiber before it was mixed into the matrix (see Figure 9).

Observation of Fiber Distribution by Optical Microscope Imaging

An optical microscope (Nikon Epiphot Metallograph) was used to obtain images of polished specimen cross-sections at low magnifications (100×) in order to observe the distribution of fibers throughout the matrix. Figure 10 shows a cross-section from the specimen reinforced with 7-mm long PVA fibers at volume fraction of 4%. It can be seen that most of the fibers are perpendicular to the cross-section. This indicates that the fibers are more or less aligned along the direction of the specimen length. The figure also illustrates the inability of the fibers to disburse within a closely spaced aggregate and suggests that the use of a smaller-sized aggregate may improve fiber dispersion.

To study the distribution of fibers throughout the matrix, analysis of polished cross-sectional images taken with the optical microscope was performed. The methodology paralleled that of Hackett and Slattery

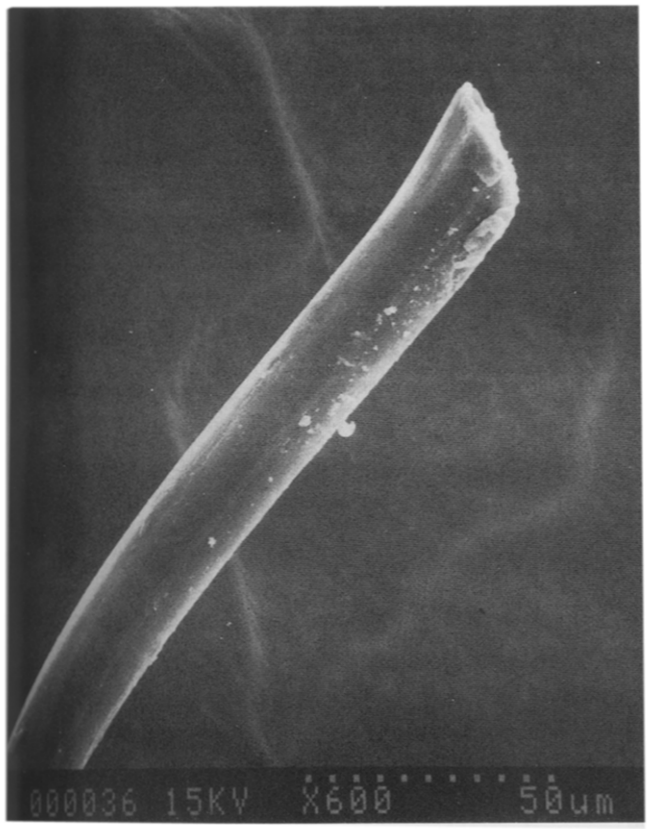

FIGURE 9. PVA fiber before it is mixed into the matrix (600× magnification).

[9]. Briefly, the location of each fiber within an image was digitized and the distances to the nearest two, three, or four fibers were calculated based on the classification of a fiber as a corner, edge, or internal fiber, respectively (see Figure 11). With this information, fiber distance cumulative distribution curves were constructed and analyzed. Fiber distance is defined as the distance between any two fibers within a plane cross-section of matrix. This fiber distance is meaningful only if the fibers are more or less aligned. On the other hand, the fiber distance is influenced by the presence of aggregates. More study on this influence is needed.

Once data processing had been completed for all three images of a particular cross-section, the fiber data from each of the three images were merged together for data analysis.

Figure 12 contains three cumulative distribution curves. One curve is from the specimen reinforced with a 4% fiber volume fraction of 4-mm long fiber. Another curve is from the specimen reinforced with a 4% fiber volume fraction of 12-mm long fiber. The third curve is from the specimen reinforced with a hybrid system of fibers composed of 2% of the 4-mm fiber and 2% of the 12-mm fiber. As is illustrated, the cumulative distribution curve of the hybrid specimen falls between the other two curves but is closer to the curve for the 4-mm fiber. Hence, the fiber distances of the hybrid system take on values that lie between those values of its independent fiber systems.

Relationship Between Fiber Distance and First Peak Stress

In an effort to determine the relationship between fiber distance and first peak stress, the fiber distance corresponding to the 95th percentile was identified for each specimen.

This fiber distance, termed the maximum fiber distance in this study, was then used to construct a plot of the experimentally measured values of first peak stress versus the corresponding maximum fiber distance for each specimen (see Figure 13). It is evident from the figure that first peak stress is a different function of maximum distance for different fiber lengths. This may be due to the fact that maximum fiber distance primarily accounts for the effect of fiber volume fraction and not fiber length and diameter. Therefore, the values of first peak stress should be normalized by a factor accounting for fiber length and diameter for comparison purposes.

In fiber-reinforced matrices, the fibers usually provide bridging across the cracked surfaces of the matrix. Because the resulting bridging force can be evaluated by pulling a fiber out from the matrix, it may be reasonable to assume that the first peak stress is proportional to the fiber pull-out force. As a result, the normalized factor for the fiber length effect on the first peak stress can be derived based on the fiber pull-out force. In a study undertaken by Stang et al [10], a relationship between the fiber pull-out force and the fracture surface energy of fiber-matrix interface was proposed. Recently, Ouyang et al. [11] have used this relationship to evaluate the peak pull-out forces of different lengths of fiber. They discovered that since the value of slip corresponding to the peak pull-out load is small, the effect of frictional stress before the peak pull-out load may be neglected. After neglecting the frictional stress, the peak pull-out force proposed by Stang et al. [10] is

$$P_c^2 = \frac{8\Gamma E_f \pi^2 r^3}{\coth^2[\omega(L - a_c)]} \tag{1}$$

where P_c is the peak pull-out force, Γ is the surface energy for debonding, r is the radius of the fiber, ω is the interfacial material parameter, L is the embedment length of the fiber, and a_c is the debonded length corresponding to the peak pull-out force. Therefore, the ratio of pull-out forces for two different fibers is

Advn Cem Bas Mat
1995;2:53–61

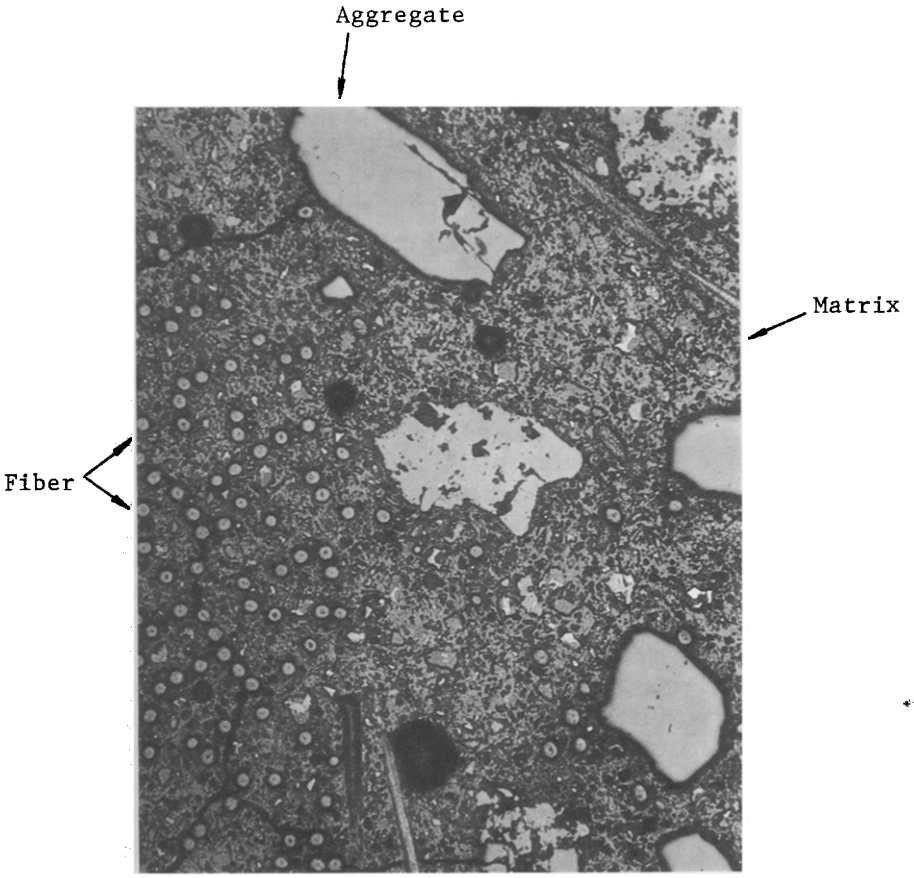

FIGURE 10. Cross-sectional image with a 4% volume fraction of 7-mm long fiber (100× magnification).

$$k_{12} = \frac{P_{c1}}{P_{c2}} = \left(\frac{r_1}{r_2}\right)^{3/2} \frac{\coth[\omega(L_2 - a_{c2})]}{\coth[\omega(L_1 - a_{c1})]} \quad (2)$$

where k_{12} is the length and diameter factor of the fibers, and subscripts *1* and *2* represent two fibers of the same type which may have different geometry and embedment lengths. It is assumed that the value of ω is equivalent for the same type of fiber and matrix. In this investigation, a value of $\omega = 133\ m^{-1}$, measured from the pull-out tests (see Table 3), was used. In addition, the value of the critical debonded length a_c was assumed to be $0.8L$ for simplicity.

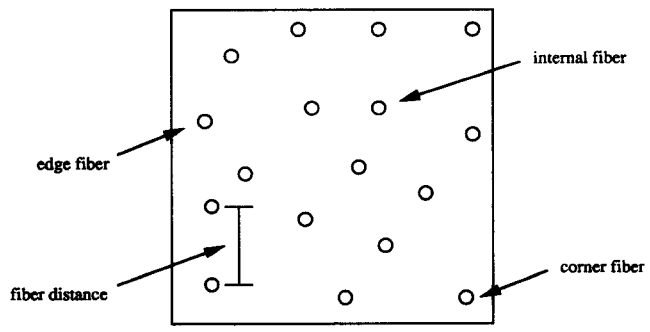

FIGURE 11. Classification of fibers for fiber distance analysis.

To compute the pull-out force ratios for the fibers used in this investigation, the 4-, 7-, and 12-mm fibers were designated as fibers *1*, *2*, and *3*, respectively. In addition, the 4-mm fiber was used as the reference fiber for comparison purposes. Hence, $k_{11} = 1$. By substituting values of r, L, and ω for the three different fibers into eq 2, values of $k_{12} = 0.203$ and $k_{13} = 0.054$ were obtained. The values of first peak stress for the

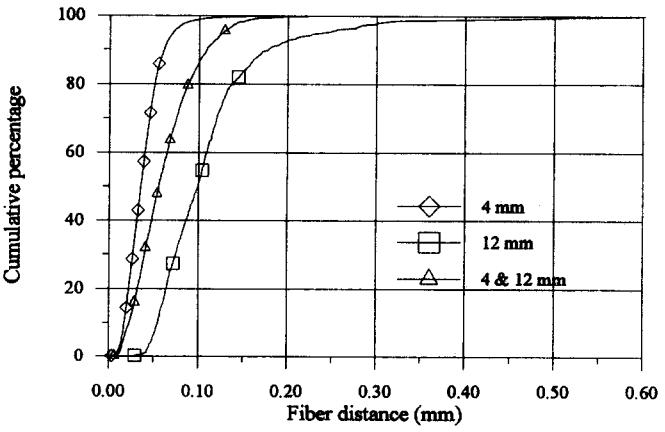

FIGURE 12. Fiber distance cumulative distribution curves for 4% fiber volume fraction of mono and hybrid systems.

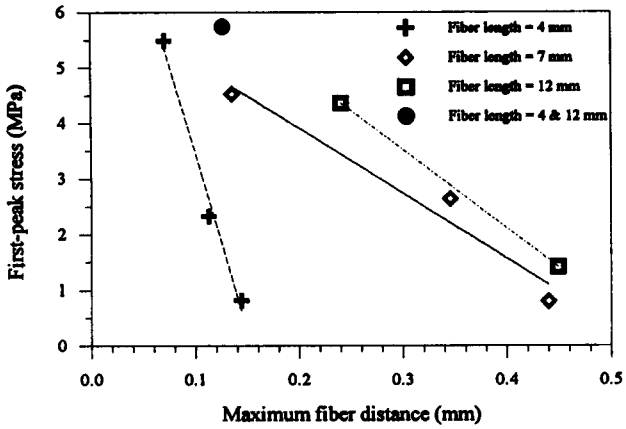

FIGURE 13. First peak stress versus maximum fiber distance.

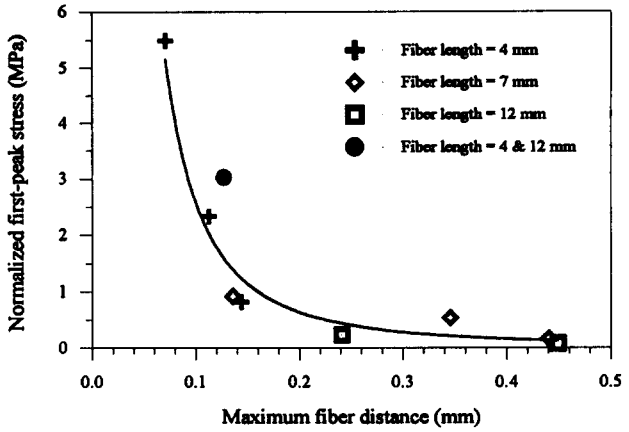

FIGURE 14. Normalized first peak stress versus maximum fiber distance.

specimen reinforced with 7-mm fiber were then multiplied by the factor $k_{12} = 0.203$, whereas the values of first peak stress for the specimens reinforced with 12-mm fiber were multiplied by the factor $k_{13} = 0.054$. For the specimen reinforced with a hybrid fiber system (2% of the 4-mm fiber and 2% of the 12-mm fiber), a normalized factor, $(1 + k_{13})/2$, equaling the average factor of its independent fiber constituents was incorporated. The resulting values of normalized first peak stress were then plotted against maximum fiber distance as shown in Figure 14. From this figure, it is evident that the normalized first peak stress can be expressed as a unique function of maximum fiber distance, regardless of the fiber length and volume fraction.

Conclusions

The experimental results indicate that the first peak stress increases with increasing fiber volume fraction as well as a decrease in fiber diameter for a constant fiber aspect ratio. On the other hand, the strain energy density increases with an increase in fiber volume fraction as well as an increase in fiber diameter. In addition, a hybrid fiber system containing 4- and 12-mm long fibers exhibited a slightly higher value of the first peak stress but a considerably higher increase in strain energy density when compared with the specimen made with single-length fiber.

The maximum pull-out load for PVA fiber occurs at much higher levels of slip than for steel fibers. This phenomenon leads to a much higher specific bond energy for the PVA fiber. When the PVA fiber is compared with polypropylene and nylon fibers, there is a similarity in their pull-out load-slip curves.

It was also found that normalized first peak stress can be related to the fiber distance with a unique function, regardless of fiber geometry and volume fraction.

Acknowledgments

Support from the National Science Foundation Center for Science and Technology of Advanced Cement Based Materials (ACBM) is gratefully appreciated. This article is based upon the first author's M.S. thesis, which was supported under a National Science Foundation Graduate Fellowship. Special acknowledgements and thanks are due to Dr. K. Shibatani of Kuraray Co., Ltd. (Osaka, Japan), who provided the specially made PVA fibers used in this research project. Dr. Z. Li is acknowledged for help on the pull-out test.

References

1. Shah, S.P.; Ouyang, C. *J. Am. Ceram. Soc.* **1991,** *74,* 2727–2953.
2. Shah, S.P. *Am. Concr. Ins. Mater. J.* **1991,** *88,* 595–602.
3. Mobasher, B.; Stang, H.; Shah, S.P. *Cem. Concr. Res.* **1990,** *20,* 665–676.
4. Banthia, N.; Sheng, J. *Mater. Res. Soc. Symp. Proc.* **1990,** *211,* 25–32.
5. Wang, Y.; Li., L.C.; Backer, S. *International Journal of Cement Composites and Lightweight Concrete* **1988,** *10,* 145–149.
6. Nanni, A.; Meamarian, N. *Cem. & Concr. Composites* **1991,** *13,* 107–114.
7. Ouyang, C.; Shah, S.P. *Cem. Concr. Res.* **1992,** *22,* 1201–2115.
8. Li, Z.; Mobasher, B.; Shah, S.P. *J. Am. Ceram. Soc.* **1991,** *74,* 2156–2164.
9. Hackett, R.M.; Slattery, K.T. *J. Mater. Civil Engin.* **1992,** *4,* 196–211.
10. Stang, H.; Li, Z.; Shah, S.P. *J. Engin. Mechanics* **1990,** *116,* 2136–2150.
11. Ouyang, C.; Pacios, A.; Shah, S.P. *J. Engin. Mechanics* **1994,** *6,* in press.